DOI: 10.1002/asia.201301398

Janus Nanoparticles: Preparation, Characterization, and Applications

Yang Song and Shaowei Chen*[a]

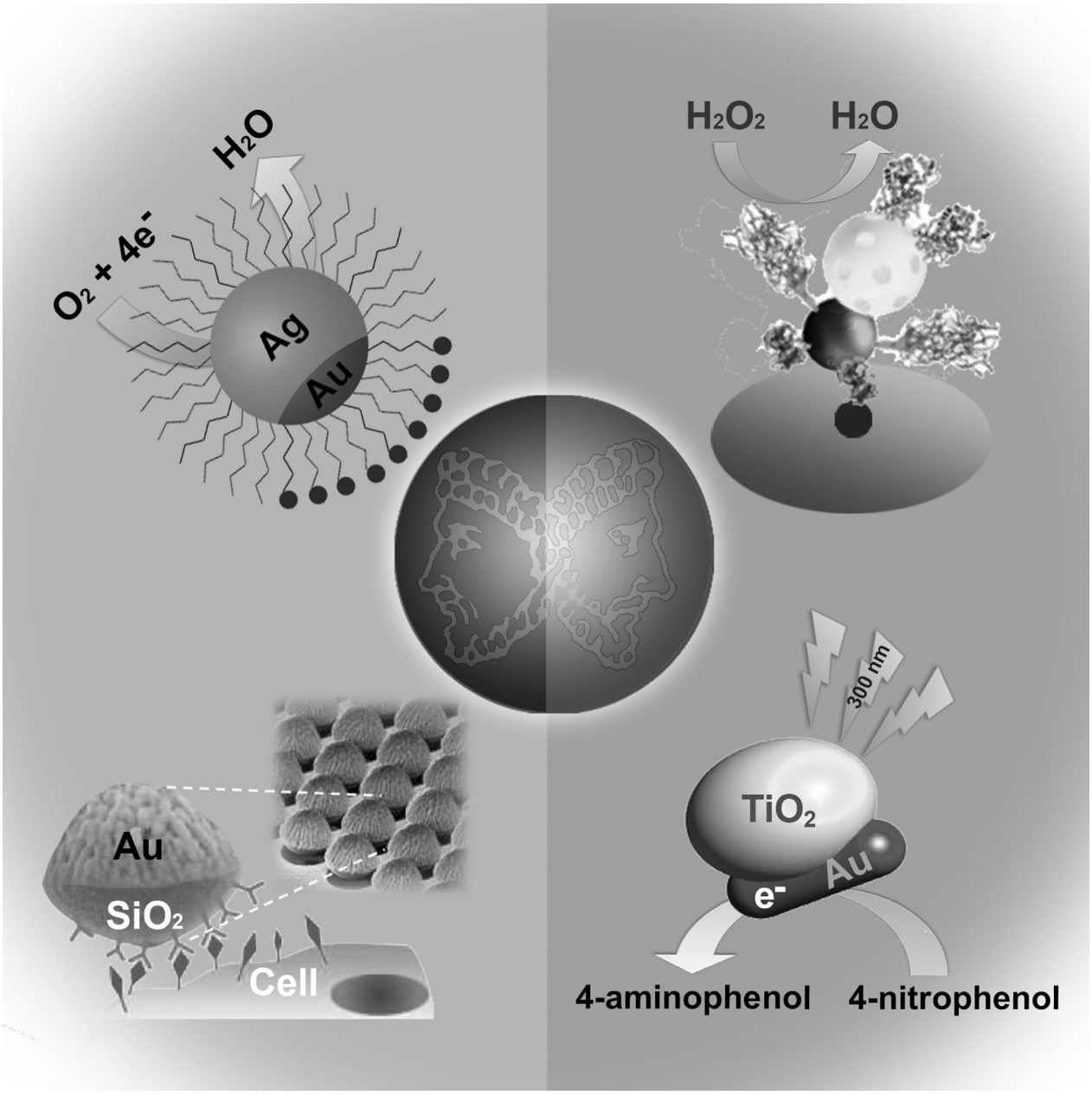

Abstract: In chemical functionalization of colloidal particles, the functional moieties are generally distributed rather homogeneously on the particle surface. Recently, a variety of synthetic protocols have been developed in which particle functionalization may be carried out in a spatially controlled fashion, leading to the production of structurally asymmetrical particles. Janus particles represent the first example in which the two hemispheres exhibit distinctly different chemical and physical properties, which is analogous to the dual-faced Roman god, Janus. Whereas a variety of methods have been reported for the preparation of (sub)micron-sized polymeric Janus particles, it has remained challenging for the synthesis and (unambiguous) structural characterization of much smaller nanometer-sized Janus particles. Herein, several leading methods for the preparation of nanometer-sized Janus particles are discussed and the important properties and applications of these Janus nanoparticles in electrochemistry, sensing, and catalysis are highlighted. Some perspectives on research into functional patchy nanoparticles are also given.

Keywords: colloids · gold · ligand exchange · nanoparticles · NMR spectroscopy

1. Introduction

Metal and semiconductor nanoparticles[1] represent a unique class of nanomaterials that show great potential as novel functional structural elements in diverse applications such as nanoelectronic devices,[2] multifunctional catalysts,[3] (bio)-chemical sensors,[4] biological labeling,[5] and data storage.[2a,6] This is largely attributable to the unique chemical and physical properties that differ vastly from those of their bulk materials and molecular species.[7] Yet, to exploit these unprecedented material properties for the fabrication of next-generation devices and circuitries, two key aspects that are intimately related to each other have to be addressed: design and synthesis of nanoscale building blocks and controlled assemblies of these structural units into functional architectures.[8] Toward this end, a great deal of research has been focused on monolayer-protected nanoparticles.[1] Here, the chemical and physical properties of the particles are the combined consequence of the inorganic cores and the organic protecting shells; more importantly, the properties of the materials can be readily manipulated by surface place-exchange reactions whereby multiple functional moieties can be incorporated into the particle protecting layer and serve as a starting point for more complicated chemical decorations.[9] Consequently, the particles behave as multifunctional reagents. Such unique properties have been demonstrated extensively by alkanethiolate-protected gold (AuSR) nanoparticles, which undergo exchange reactions with other thiol derivatives by taking advantage of the strong affinity of thiols to gold surfaces (Figure 1a; the resulting particles are denoted as bulk-exchange particles because the reactions typically occur with the particles and the incoming ligands dispersed in the same solvent media).[9c–e,10] More recently,

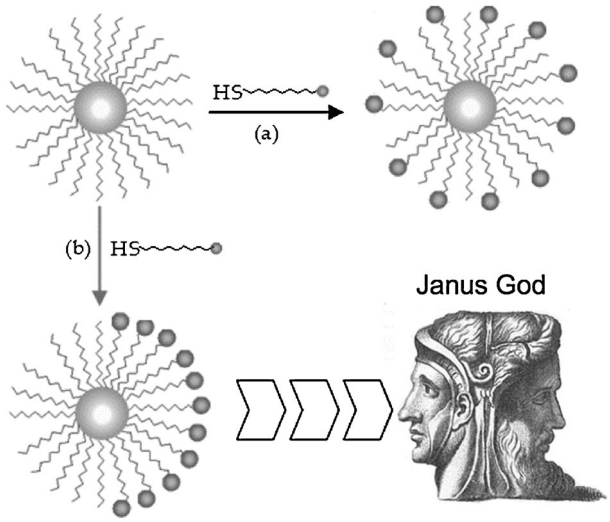

Figure 1. Schematic representation of surface functionalization based on ligand-exchange reactions for the production of a) bulk-exchange and b) Janus nanoparticles.

we demonstrated that, for carbene- or alkyne-functionalized metal nanoparticles,[11] olefin metathesis reactions on the surface of the nanoparticle with other vinyl- or acetylene-terminated derivatives could also be exploited for particle surface functionalization.

To further and better control the assembly of these nanoscale building blocks into functional architectures, it is of critical importance to look for additional parameters beyond size and shape for the design of the nanomaterials. Among these, of particular interest is the creation of amphiphilic nanoparticles that exhibit hydrophobic characters on one side and hydrophilic on the other, akin to the dual-faced Roman god, Janus (hence, Janus nanoparticles, as suggested by de Gennes, Figure 1b).[12] These particles represent a unique nanoscale analogue to conventional surfactant molecules, and thus, may be exploited in the formation of functional superstructures by virtue of self-assembly.[13] Such supraparticular assemblies[14] will not be accessible with homogeneously functionalized building blocks,[15] and thus,

[a] Y. Song, Prof. S. Chen
Department of Chemistry and Biochemistry
University of California, 1156 High Street
Santa Cruz, California 95064 (USA)
Fax: (+1) 831-459-2935
E-mail: shaowei@ucsc.edu

offer a novel paradigm to the rational design and preparation of functional ensembles.

Yet, most prior research focused on (sub)micron-sized Janus particles based on polymeric materials. Several effective routes have been reported towards the synthesis of these biphasic particles.[15c,16] For instance, microfluidic flow systems have been used to prepare amphiphilic particles by the polymerization of the Janus droplets formed within the microfluidic channels.[14b,15c] Submicron-sized Janus particles were also prepared by biphasic electrified jetting of two polymer precursors.[16b] In another report, Suzuki and Kawaguchi demonstrated that Janus particles could be produced by sputtering gold onto the top face of a polymer bead array upon which further functionalization on the gold surface might be achieved.[16c] Additionally, Paunov and Cayre reported the fabrication of Janus particles by the replication of particle monolayers at liquid surfaces by using a gel trapping technique.[17]

For bare colloids, research into Janus particles has mostly focused on bicompartmental structures. A typical synthetic procedure involves partial masking of the surfaces of the particles prior to selective engineering and functionalization of the exposed particle surfaces.[18] These include surface coating by vapor deposition of metal thin films/particles,[16c,19] spin-coating of a photoresistant layer and metal evaporation,[20] electrostatic deposition,[21] layer-by-layer self-assembly,[14a,22] polymer self-assembly,[23] surface-initiated free-radical polymerization,[24] photo-polymerization in a microfluidic channel,[25] the Pickering emulsion method,[26] biphasic electrified jetting,[16b,27] protonation–deprotonation cycling,[28] in situ click chemistry,[29] and chemical modification.[30]

Abstract in Chinese:

在胶体粒子的化学功能化中，官能基团一般都相当均匀地分布在颗粒表面上。最近一段时间，文献中报道了多种合成途径以对纳米颗粒的功能化进行空间控制，生成结构不对称颗粒。两面神粒子就是其中一个有代表性的例子。这种粒子在两个半球表现出明显不同的化学和物理性质，结构上类似于罗马神话中的两面神。虽然基于微米尺寸的聚合物两面神粒子已经有诸多报道，更小的纳米尺寸的两面神粒子的合成和结构表征仍然有相当大的困难。在这篇重点综述中，我们将着重讨论一些制备两面神纳米粒子的有效方法，然后突出这些纳米粒子在电化学，传感和催化反应上的重要性质和应用研究，并对更复杂的补丁纳米粒子的前景作些展望。

In these studies, it has been demonstrated that Janus particles with oppositely charged hemispheres exhibit a large dipole moment, which may be exploited for remote positioning in an electric field.[17,19b,c,31] When the Janus particles have both electrical and color anisotropy, they may be used in electronic paper.[32] Janus particles coated with different chemical groups can also be derivatized into bifunctional carriers that are useful for catalysis, sensing, drug delivery, and so forth.[33] Janus particles with an electron-donor side and an -acceptor side may also be exploited as nanoscale machinery in the conversion of solar energy into electrical currents.[33] The amphiphilic Janus particles with hydrophilic and -phobic hemispheres can also be used as particular surfactants in the stabilization of water-in-oil or oil-in-water emulsions,[16a,34] in contrast to the homogeneously functionalized counterparts.[35] In addition, they can self-organize and select left from right, or top from bottom, to yield supraparticular architectures in a preprogrammed fashion.[36]

Janus particles also show potential applications in catalysis, sensing, and drug delivery by deliberate and independent decoration of the two hemispheres with different chemical functional moieties.[37] Moreover, Janus particles may be exploited to control molecular recognition and self-assembly processes, which represent some of the most intriguing and challenging aspects of materials science research.[38]

It should be noted that, in these earlier studies, the typical particle sizes range from a few hundred nanometers to a few micrometers. Several review articles have emerged that are primarily focused on the synthesis and/or self-assembly of

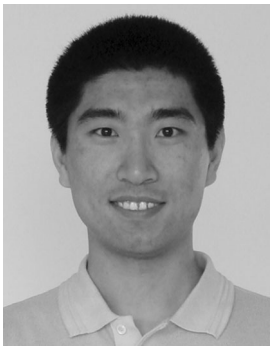

Yang Song received his B.Sc. degree in chemistry from Jilin University in 2005 and his M.Sc. degree in nanomaterials from Shandong University under the co-supervision of Profs. Dairong Chen and Xiuling Jiao in 2008. He then started his PhD studies at the University of California, Santa Cruz, under the supervision of Prof. Shaowei Chen. His current research interests focus on the synthesis of metallic Janus nanostructures and exploring their (electro)chemical and catalytic applications.

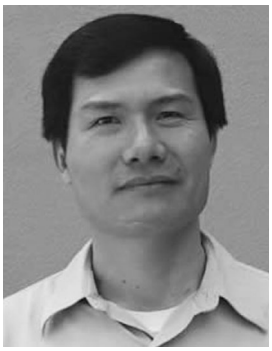

Shaowei Chen finished his undergraduate studies in China in 1991 with a B.Sc. degree in chemistry from the University of Science and Technology of China, and then went to Cornell University, receiving his M.Sc. and Ph.D. degrees in 1993 and 1996, respectively. Following a postdoctoral appointment at the University of North Carolina at Chapel Hill, he started his independent career in Southern Illinois University in 1998. In summer 2004, he moved to the University of California at Santa Cruz and is currently a Professor of Chemistry. His research interest is primarily in the electron transfer chemistry of nanoparticle materials.

polymeric and oxide colloidal Janus particles,[16a,18a–d] and the design and fabrication of other patchy and multicompartmental structures.[18e–g,39] However, reports on the synthesis of nanometer-sized Janus particles are actually rather scarce.[30] In fact, the majority of nanometer-sized Janus particles refer to bifunctional heterodimers that consist of two different materials segregated in the particle cores, forming snowman or dumbbell-like nanostructures,[40] whereas only a limited number of studies are focused on Janus nanoparticles with two types of organic capping ligands segregated on the two hemispheres of the nanoparticles.

In addition, for (sub)micron-sized Janus particles, the structural asymmetry may be directly visualized with the aid of a conventional electron microscope. Yet, for much smaller, nanometer-sized Janus particles, unambiguous characterization and verification of the amphiphilic structures has become much more challenging. Therefore, herein, we first summarize several leading methods for the preparation and characterization of organically capped metal Janus nanoparticles and then highlight some recent progress in the further functionalization and engineering of Janus nanoparticles and their electrochemical and catalytic properties. We conclude this review with some perspectives on the research and development of functional patchy nanoparticles.

2. Interfacial Engineering

In contrast to the micron-sized counterparts, the choices of synthetic protocols for nanometer-sized Janus nanoparticles are rather limited. Langmuir-based methods have been adopted as an effective way for the production of Janus nanoparticles that exhibit hydrophobic characters on one side and hydrophilic on the other.[41] Recently, we developed two effective strategies based on interfacial engineering for the preparation of Janus nanoparticles. The first method is depicted in Figure 2.[41,42] In this study, *n*-hexanethiolate-capped gold nanoparticles (AuC6; average core diameter 2 nm with ≈15% core size dispersity, as determined by TEM measurements) were used as the starting materials. Experimentally, the amphiphilicity was rendered to the AuC6 nanoparticles by subjecting them to ligand-exchange reactions with hydrophilic 3-mercaptopropane-1,2-diol (MPD) at the air|water interface at a sufficiently high surface pressure by mechanical compression.

In the second approach (Figure 3),[43] a monolayer of AuC6 nanoparticles was first deposited onto a substrate surface by the Langmuir–Blodgett (LB) technique at a sufficiently high surface pressure, at which ligand intercalation between adjacent nanoparticles occurred. The sample was then immersed into an aqueous solution of hydrophilic ligands, such as 2-(2-mercaptoethoxy)ethanol (MEA), in which the ligand-exchange reactions were limited to the top face of the nanoparticles, and thus, leading to the formation of Janus nanoparticles. With this experimental setup, the exchange dynamics might also be readily assessed by contact angle measurements.

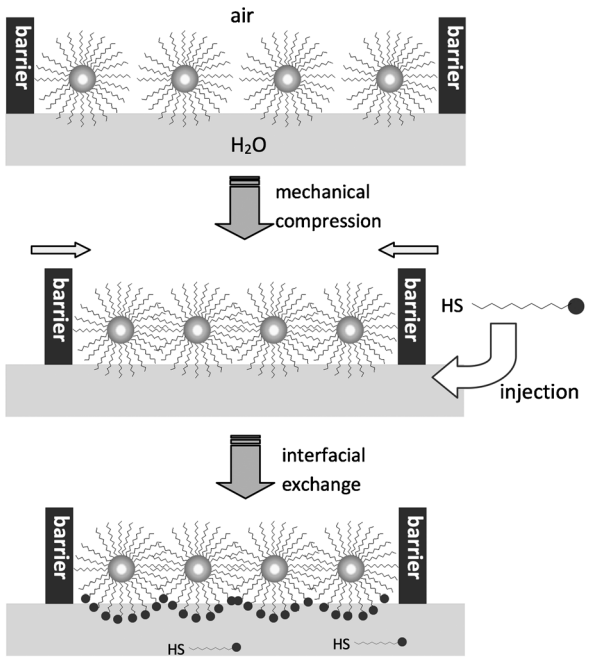

Figure 2. Schematic representation of the preparation of Janus nanoparticles based on the Langmuir technique. Reprinted with permission from ref. [41]. Copyright 2007 Wiley.

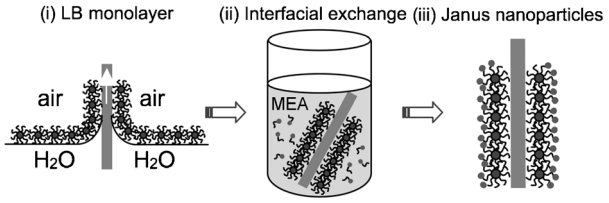

Figure 3. Schematic representation of the synthesis of Janus nanoparticles by using nanoparticle monolayers prepared by the LB method. MEA = 2-(2-mercaptoethoxy)ethanol. Reprinted with permission from ref. [43]. Copyright 2009 Springer.

The amphiphilic nature of the resulting Janus nanoparticles was confirmed by a variety of experimental tools, including contact angle measurements of nanoparticle monolayers (ensembles) as well as adhesion force studies of individual nanoparticles.[41,42] In addition, NMR spectroscopic measurements have also been carried out for the quantitative assessment of the surface composition and ligand distribution of the Janus nanoparticles. Figure 4A, top, depicts a representative ^{1}H NMR spectrum of the AuC6–MEA Janus nanoparticles in $CDCl_3$. The signal at $\delta = 0.90$ ppm is ascribed to the protons of the terminal methyl group of the hexanethiolate ligands, whereas the broad signals at $\delta = 3.60$ and 3.80 ppm are attributable to the methylene protons next to the hydroxyl (OH) group and the ether group in the MEA ligands, respectively. From the ratio of the integrated peak areas of these protons, it can be estimated that 44.6% of the original hexanethiolate ligands were replaced by the MEA ligands in the Janus particles. In a similar fashion, for the bulk-exchanged particles prepared by mixing the AuC6 nanoparticles and MEA in THF for ligand-exchange reac-

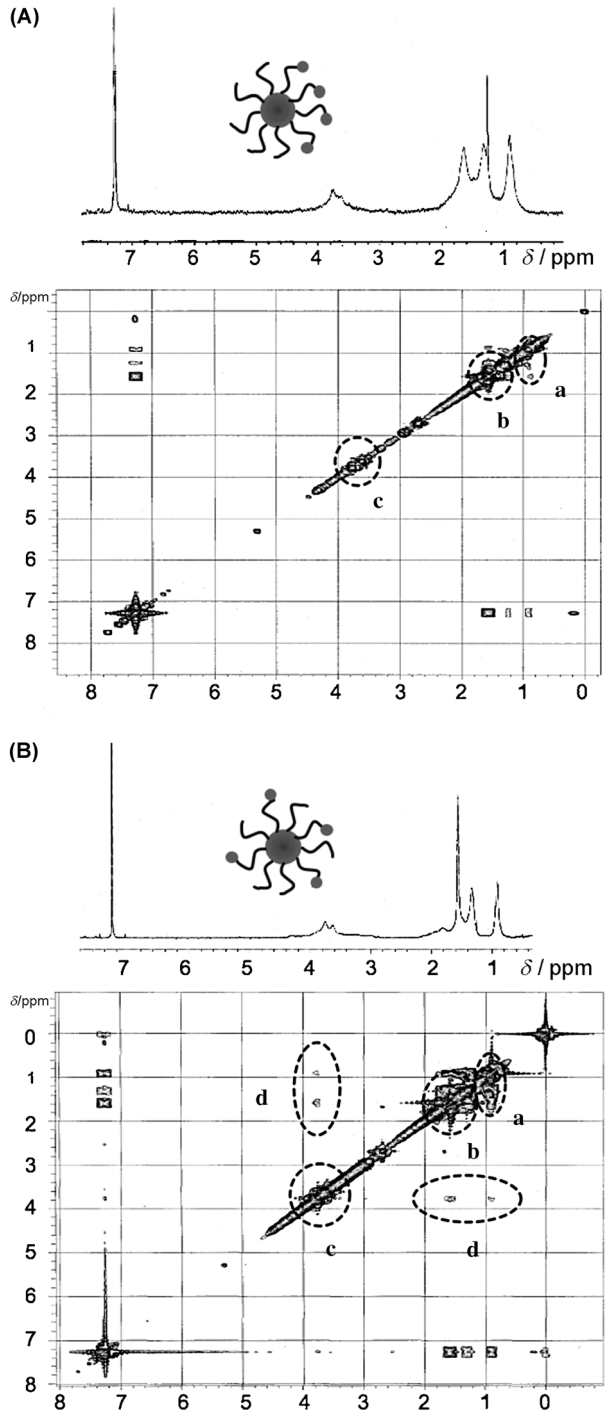

Figure 4. The ^{1}H (top) and NOESY (bottom) NMR spectra of A) the Janus and B) bulk-exchanged nanoparticles in $CDCl_3$. The corresponding NOESY NMR spectra were acquired with a mixing time of 120 ms. Circles highlight the cross peaks between the protecting ligands on the particle surface. Insets show the respective schematic of the nanoparticles. Reprinted with permission from ref. [43]. Copyright 2009 Springer.

tions, the protecting monolayer was found to consist of 51.2% MEA and 48.8% hexanethiolate (Figure 4B, top). Both results suggest an approximately equal number of hydrophobic and -philic ligands on the nanoparticle surface, that is, they are equivalent to structural isomers.

To further establish the amphiphilic characters of the Janus nanoparticles, we also employed NOESY spectroscopy to examine the spatial correlation between nuclear spins,[43] which we believe is the first of its kind in the investigation of Janus nanoparticles at the molecular level. NOESY is a two-dimensional NMR spectroscopy technique in which cross peaks arise from dipole–dipole interactions (i.e., through-space coupling) between nuclear spins that are in close proximity (typically <0.4 nm) because the intensity of the cross peaks depends inversely on the sixth power of the distance between the protons.[44] These unique features can thus be exploited to estimate the internuclear distance and, for monolayer-protected nanoparticles, a quantitative assessment of the packing (distribution) of organic capping ligands on particle surfaces.[45]

Figure 4 depicts the corresponding NOESY spectra for the AuC6-MEA Janus (A, bottom) and bulk-exchanged particles (B, bottom). The diagonal profiles of both spectra indicate apparent polarization interactions between adjacent spins from both intra- and interchain contributions.[43] Of these, the peaks in circles a in Figure 4 can be ascribed to the interactions between the methyl protons and between the methyl and methylene protons of the hexanethiolate ligands, the peaks in circles b reflect the interactions between the methylene protons from the hexanethiolate ligands, whereas those in circles c are from the MEA ligands. In addition to these common features, remarkable discrepancy can also be observed. The most significant difference between these two spectra is the appearance of two cross peaks between the methyl/methylene protons of the hexanethiolate ligands and the methylene protons of the MEA ligands for the bulk-exchanged particles, which are highlighted in circles d in Figure 4B. Notably, these cross peaks are totally absent in the Janus particles (Figure 4A). Such an observation is consistent with the structural models for the surface distribution of the two types of ligands on the nanoparticle surface (Figure 4, insets). In the Janus nanoparticles, the absence of these cross peaks clearly indicates that the hexanethiolate ligands are segregated from the MEA ligands, that is, these two ligands are situated on two different hemispheres of the nanoparticle surface. In contrast, in the bulk-exchanged particles, the cross peaks were observed because of the homogeneous mixing of the two ligands, and hence, extensive interactions between the neighboring ligand protons.[46]

From the above studies, we can see that 1) interfacial engineering (Figures 2 and 3) is indeed an effective route to the preparation of amphiphilic Janus nanoparticles, and 2) the structural asymmetry can be quantified on multiple length scales, ranging from contact angle measurements of nanoparticle organized ensembles, to adhesion force studies of individual nanoparticles, and to NOESY NMR spectroscopy measurements of nuclear spin interactions between capping ligands.

With the asymmetric surface chemistry, the amphiphilic Janus nanoparticles indeed behave analogously to conventional surfactant molecules in the formation of superparticu-

lar assemblies, yet with a critical micelle concentration of several orders of magnitude lower, as manifested in Raman spectroscopic and dynamic light scattering measurements.[47]

Yet, the structure stability of Janus nanoparticles may be compromised, owing to diffusion of thiol ligands on metal surfaces even at room temperature, leading to eventual homogeneous mixing between the hydrophobic and -philic ligands on the Janus nanoparticle surface.[48] Thus, to enhance the nanoparticle structural integrity, covalent cross-linking between neighboring organic ligands has been exploited to impede diffusion of thiol ligands on gold nanoparticle surfaces, as exemplified by UV photo-polymerization of diacetylene moieties embedded within the ligand chemical backbones (Figure 5).[49]

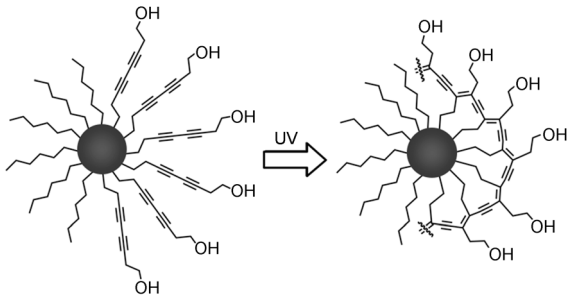

Figure 5. Covalent cross-linking of surface capping ligands of Janus nanoparticles by UV polymerization of diacetylene moieties. Reprinted with permission from ref. [49]. Copyright 2011 American Chemical Society.

3. Janus Heterodimers

The asymmetric surface chemistry of the Janus nanoparticles may then be used as new anchoring points for more complicated surface functionalization.[9a,e,50] For instance, Au–TiO_2 snowman-like heterodimers (Figure 6) derived from Janus gold nanoparticles have been prepared by a surface sol–gel process based on gold Janus nanoparticles, the surface-protecting monolayers of which consisted of a hemisphere of hydrophobic 1-hexanethiolates and the other of hydrophilic MEA.[47b] TEM measurements showed that the resulting TiO_2 nanoparticles (diam 6 nm) exhibited well-defined lattice fringes that were consistent with the (101) diffraction planes of anatase TiO_2. The heterodimer nanoparticles displayed apparent photoluminescence that was ascribed to electronic transitions involving trap states of TiO_2 particles, and the photocatalytic activity was manifested by the oxidative conversion of methanol into formaldehyde, which was detected quantitatively by the Nash method. The enhanced photocatalytic performance, compared with that of P25 TiO_2 colloids, was ascribed to the charge separation of photogenerated electrons and holes at the Au–TiO_2 interface facilitated by the close proximity of the gold nanoparticles. These results suggested that 1) there were at least two possible pathways for photogenerated electrons at the TiO_2 conduction band: decay to the trap states and transfer to the gold nanoparticles, and 2) energy/electron transfer from the trap

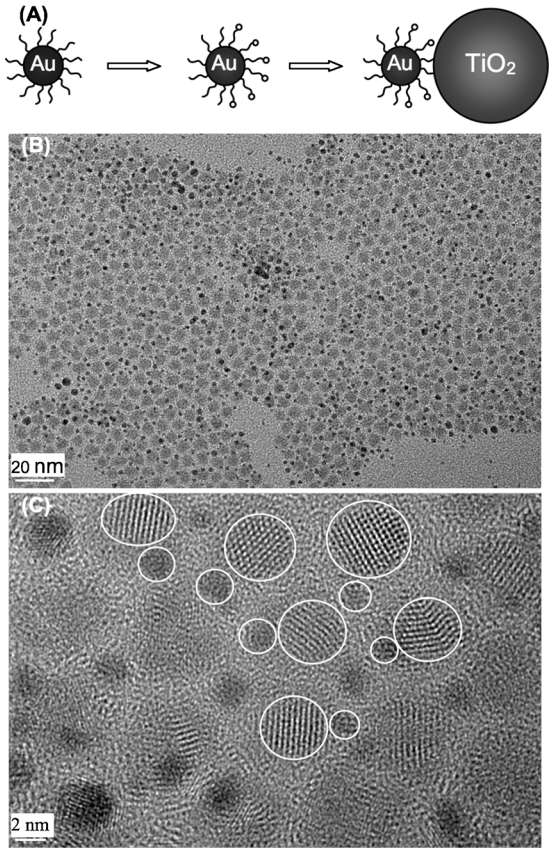

Figure 6. A) Schematic representation of the preparation of Au–TiO_2 heterodimer nanoparticles. B) and C) TEM micrographs of Au–TiO_2 heterodimer nanoparticles. The scale bar is 20 nm in B) and 2 nm in C). The lattice fringes of TiO_2 in panel C) exhibit a lattice spacing of 0.36 nm, corresponding to the (101) diffraction planes of anatase TiO_2. Reprinted with permission of ref. [47b]. Copyright 2009 American Chemical Society.

states to gold nanoparticles was less efficient. In essence, this study showed that the snowman-like heterodimers might be exploited as a homogeneous photocatalytic system for the preparation of functional molecules and materials.

Much larger Janus-like Au (diam $\approx$50 nm)–TiO_2 (diam $\approx$100 nm) heterodimers have also been prepared by using a block copolymer template, and exhibited apparent photocatalytic activity for efficient hydrogen generation under visible-light photoirradiation[51] and methylene blue degradation,[52] owing to their strong localization of plasmonic near-fields close to the Au–TiO_2 interface. In this region, the plasmonic near-fields are strongly coupled to optical transitions involving localized electronic states in amorphous TiO_2, leading to enhanced optical absorption and the generation of electron–hole pairs for photocatalysis.

In another study, Seh et al. reported the anisotropic growth of TiO_2 (diam $\approx$50 nm) onto gold nanorods, resulting in the formation of Janus, eccentric core–shell, and concentric core–shell nanostructures that may be used to catalyze 4-nitrophenol reduction with high cyclic stability.[53] The morphology of the TiO_2–Au nanorod composites was controlled by 1) the slow hydrolysis rate of titanium diisoprop-

oxide bis(acetylacetonate) (TDAA) as a titanium precursor; and 2) the amount of titanium precursor and reaction time. Because the partially hydrolyzed TDAA precursor is hydrophobic in nature and does not have good wettability on the hydrophilic surface of the hydroxypropyl cellulose capped gold nanorods, upon the rapid addition of TDAA, TiO_2 would nucleate and grow on one side of the gold nanorods as Janus TiO_2-coated gold nanorods to reduce the Au–TiO_2 interfacial area; thus enabling minimization of interfacial energy at the expense of elastic energy, owing to bending of the nanorods, as shown in Figure 7A. In comparison, increasing the amount of TDAA added led to the generation of concentric Au–TiO_2 nanostructures with uniformly thick shells on both sides of the gold nanorods. More importantly, the unique advantage of the Janus geometry lies in the exposure of the gold core on one side, which provides direct access to reactants for high catalytic rates. This has been manifested in the reduction of 4-nitrophenol to 4-aminophenol by sodium borohydride, which is known to be catalyzed by gold nanoparticles.[54] The Janus nanostructures were found to catalyze the reaction at a rate as fast as that of bare spherical gold nanoparticles during the first cycle of use (Figure 7), because the exposed gold core on one side of the Janus catalysts provides direct access to 4-nitrophenol. Yet, the Janus catalysts showed high stability with no clear diminishment in activity after five cycles, whereas the catalytic activity of unprotected bare gold nanoparticles was reduced to almost zero after five cycles owing to irreversible aggregation. This could be ascribed to the presence of TiO_2 coatings that protect against aggregation.

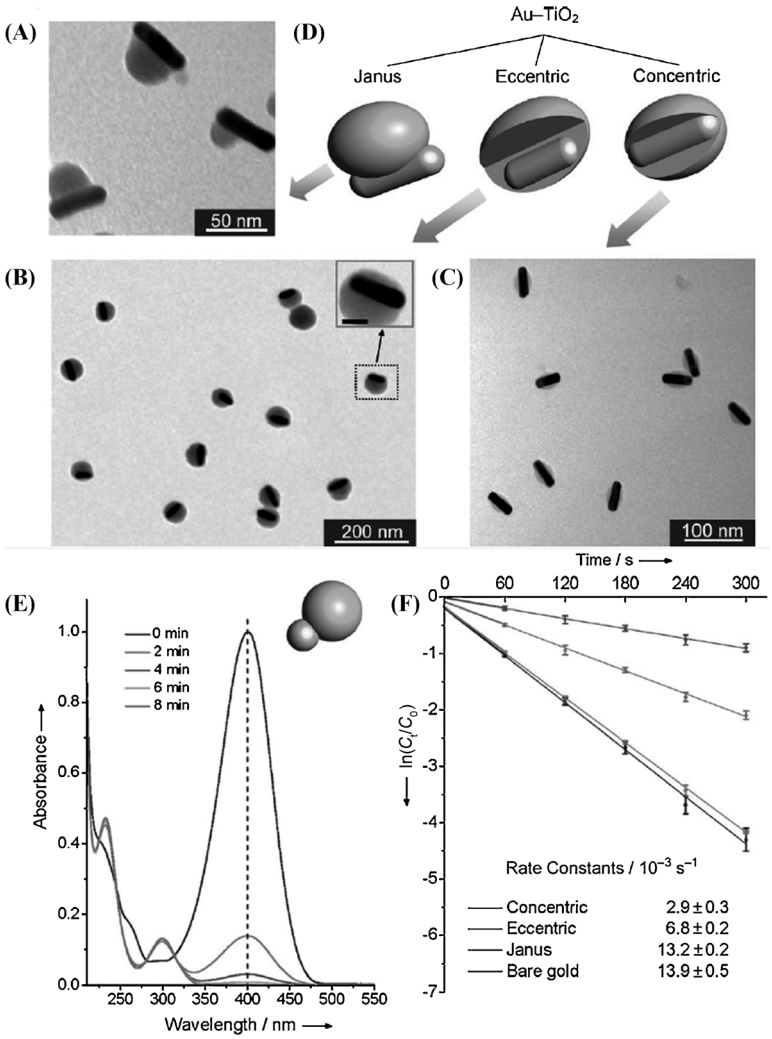

Figure 7. TEM images of TiO_2-coated short gold nanorods with A) Janus, B) eccentric, and C) concentric geometries. The inset in B) shows a thinner TiO_2 shell on one side and a thicker one on the opposite side (scale bar 25 nm). D) Schematic representations of the TiO_2-coated short gold nanorods with various geometries. E) Time-dependent evolution of UV/Vis absorption spectra of the catalytic reduction of 4-nitrophenol to 4-aminophenol by sodium borohydride during the first cycle of using the Janus TiO_2-coated spherical gold nanoparticles. F) Plots of $\ln(C_t/C_o)$ versus time and the rate constants for bare and TiO_2-coated spherical gold nanoparticles with various geometries. The concentration of catalysts used was kept constant at approximately 5.0×10^{10} particles mL^{-1} for all experiments. Reprinted with permission of ref. [53]. Copyright 2011 Wiley.

The preparation of other metal–semiconductor heterodimeter nanostructures has also been reported recently. For instance, Liu et al. reported the preparation of a heterodimer nanostructure by growing heavily doped p-type $Cu_{2-x}Se$ (diam 4.6–5 nm) onto Au seed nanoparticles (diam 2.6–4.6 nm).[55] The nanocomposites exhibited a broad localized surface plasmon resonance across the visible and near-infrared region, and thus, might be used for in vivo photoaccoustic imaging and in vitro dark-field imaging.

It can be envisioned that, of the metal–semiconductor heterodimers, the chemically labile component might also be used as a temporary protecting mask for the further engineering of the other component, leading to the generation of more complicated nanostructures. This has been demonstrated by Liz-Marzán and co-workers in the preparation of gold Janus stars.[56] The procedure involved four key steps: 1) citrate-capped gold spheres (40 nm in diam) were added to a solution containing 4-mercaptobenzoic acid (MBA) and poly(acrylic acid) (PAA), in which the two ligands were self-assembled onto the nanoparticle surface to form apparently segregated domains; 2) silica was then

formed by the Stöber method onto the MBA region, whereas PAA stabilized the exposed gold surface; 3) gold spikes were then grown onto the "bare" gold surface by a surfactant-free approach with ascorbic acid as the reducing reagent in the presence of $HAuCl_4$, $AgNO_3$, and HCl; and 4) the SiO_2 protecting shell was removed.

3. Electron Transfer of Janus Nanoparticles

The availability of structurally asymmetric Janus particles provides a new and powerful platform on which the nanoparticles can be engineered and functionalized to an unprecedented extent. This has been exemplified in a recent study in which bimetallic Janus nanoparticles were prepared by the interfacial engineering method and exhibited unique electrocatalytic activity in oxygen reduction; a critical reaction in fuel cell electrochemistry.[57] In this study, bimetallic silver–gold Janus nanoparticles were prepared by galvanic exchange reactions of 1-hexanethiolate passivated silver (AgC6, diam $\approx$5 nm; Figure 8A) nanoparticles with a gold(I)–mercaptopropanediol ([Au^IMPD]) complex. The experimental procedure was similar to that outlined in Figure 3. Specifically, a monolayer of the AgC6 nanoparticles were deposited onto a solid substrate surface by the LB method and then immersed into the solution of [Au^IMPD] in water/methanol (1:1 v/v). Galvanic exchange reactions were limited to the top face of the nanoparticles in direct contact with the gold(I) complex solution. The resulting nanoparticles exhibited an asymmetric distribution not only of the organic capping ligands on the nanoparticle surface, as shown by contact angle measurements, but also of the metal elements in the nanoparticle cores, in contrast to the bulk-exchange counterparts for which these distributions were homogeneous within the nanoparticles, as manifested by EDX elemental analysis in Figure 8B and C. More interestingly, despite a minimal loading of Au onto the Ag nanoparticles, the bimetallic AgAu nanoparticles exhibited enhanced electrocatalytic activity in oxygen reduction reactions, as compared with the monometallic AgC6 nanoparticles. Additionally, the electrocatalytic performance of the Janus nanoparticles was markedly better than that of the bulk-exchange ones, as shown in the Tafel plot (Figure 9) in which the kinetic current increased by the order of AgC6 < bulk-exchange < Janus nanoparticles, suggesting that the segregated distribution of the polar ligands from the apolar ones might further facilitate charge transfer from Ag to Au in the nanoparticle cores, leading to additional improvement of the adsorption and reduction of oxygen.

Metal–metal dumbbell-like nanoparticles have also been prepared in which two different metal domains are epitaxially linked with two different types of material surfaces. For instance, pear-like heterodimers and peanut- and clover-like nanosized PtAu nanostructures have been synthesized by Wang et al.[58] The shape of the nanocomposites was controlled by the intrinsic driving force for multiple and separate nucleation of gold over platinum along the <111> direction. Upon increasing size of the platinum seed particles from 3 to 7 nm, the overall energy of the platinum–gold structures became dominated by the interfacial energy that growth of gold was allowed into separate particles on multiple facets. Moreover, the resulting asymmetric nanostructures showed improved activities in methanol oxidation reactions relative to the original platinum nanoparticles. Although the mechanism is still unclear, this may be due to partial electron deficiency of platinum in the platinum–gold nanoparticles as a result of electron transfer from platinum to gold between their Fermi levels across the interface, similar to the work of bimetallic silver–gold Janus nanoparticles described above.[57] Furthermore, clover-like platinum–gold

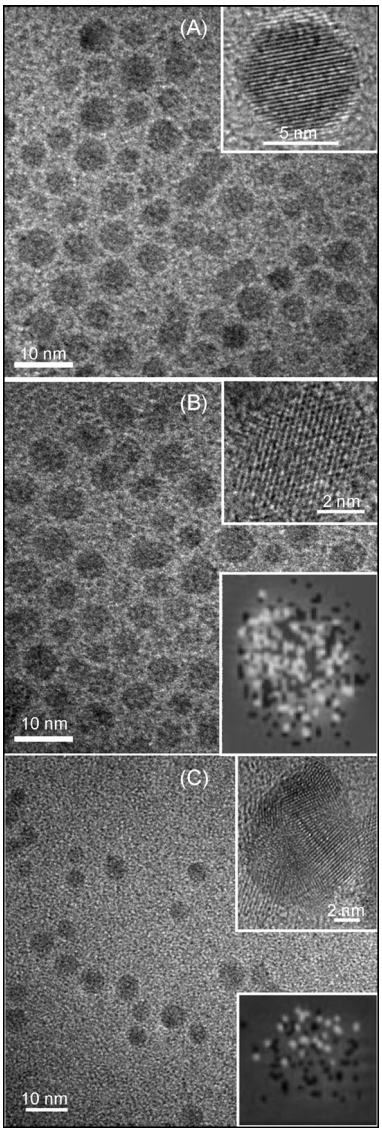

Figure 8. Representative TEM micrographs of A) AgC6, B) AgAu bulk-exchange, and C) AgAu Janus nanoparticles. Upper insets show the corresponding high-resolution TEM images. Lower insets in panels B) and C) are the representative false-color energy-dispersive X-ray spectroscopy (EDX) elemental maps of bulk-exchange and Janus nanoparticles with black symbols for Ag and white for Au. Reprinted with permission of ref. [57]. Copyright 2012 American Chemical Society.

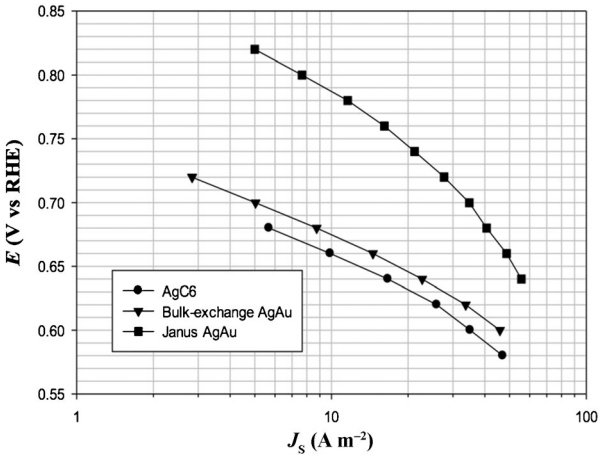

Figure 9. Tafel plots of the area-specific kinetic current densities at varied electrode potentials. Reprinted with permission of ref. [57]. Copyright 2012 American Chemical Society.

nanoparticles were found to show greater electrocatalytic activities in methanol oxidation than those of the pear-like ones, because electron transfer could be more prominent in platinum–gold with more gold branches.[59] These studies suggest that the spatial distribution of metal elements within alloy nanoparticles may be exploited as a new powerful variable in the manipulation of nanoparticle electrocatalytic activity, in contrast to conventional alloy particles in which the distribution is mostly random.

In more recent study, Wang et al. reported the preparation of metal heterostructures by using gold nanorods as the seed particles.[60] The strategy was based on a site-selective silica coating for which silica was selectively grown either on the two ends of the gold nanorods because of the higher curvature or on the side surface when the ends were protected by thiol-terminated methoxypoly(ethylene glycol). Overgrowth of another metal (e.g., Ag, Pd, and Pt) was then directed only to the exposed gold surface, forming different metal heterostructures. Nevertheless, the electron-transfer properties of such engineered nanostructures remain to be explored.

Charge transfer between the two components within Janus nanocomposites has also been found to improve the electrochemical performance of CuO–SnO_2 Janus nanorods in applications as electrode materials for lithium ion batteries.[61] These oxide composites were prepared by a one-step method based on flame spray pyrolysis. Ultrasonically generated droplets of aqueous solutions of $SnSO_4$ and $Cu(NO_3)_2$ with propane and oxygen were introduced into the flame spray pyrolysis system at a specific rate. The SnO_2 and CuO components were completely evaporated in the diffusion flame at temperatures over 2500 °C; thus forming Janus-structured composite powders from the vapors by nucleation and growth with spherical CuO deposited onto the surface of rod-shaped SnO_2 because the latter exhibited a higher melting temperature.[62] The CuO content of the composite powders was >30 wt %. The aspect ratios of the SnO_2 nanorods in the SnO_2–CuO (70/30 wt %) and SnO_2–CuO (50/50 wt %) composite powders were about four and three, respectively. The composition of Janus-structured SnO_2–CuO was also confirmed by EDX elemental mapping.[63]

Electrochemical studies were then carried out to evaluate the performance of the SnO_2–CuO composite powders as electrode materials for lithium ion batteries, for which insertion of lithium into the anode is referred to as discharging and lithium extraction from the electrodes as charging. The Janus SnO_2–CuO composite powders exhibited higher capacity retention than that of pure SnO_2 nanoparticles, which increased with increasing CuO content. For instance, pure SnO_2 showed a capacity retention of 39 % after 50 charging/discharging cycles, which doubled to 80 % for the SnO_2–CuO (70/30) composite powders and 85 % for SnO_2–CuO (50/50; note that a good cyclic performance of 392 mA h g^{-1} was also observed). It is likely that the enhanced electronic conduction and charge transfer by the high-aspect-ratio SnO_2 nanorods along the axial direction improved the electrochemical properties of the Janus-structured SnO_2–CuO composite powders.

Furthermore, the CuO nanopowders attached onto the SnO_2 nanorods were found to improve the electrochemical properties of the composite powders by increasing the electrical connection between the SnO_2 nanorods during cycling.[64] This conclusion was supported by electrochemical impedance spectroscopic measurements in which the diameter of the semicircles obtained before cycling in the medium frequency region for the SnO_2–CuO (70/30) composite electrode was smaller than that of the pure SnO_2 electrode; this indicated that the composite electrode showed lower charge-transfer impedance than that of the pure SnO_2 electrode. The reduction of the resistance can be attributed to the improved electronic conductivity of the composite electrode induced by the rod-like Janus structures. The composite powders also showed lower charge-transfer impedances than the pure SnO_2 electrodes after the 50th cycle. The improved electronic conductivity of the electrodes played a key role in the reduction of the overall resistance. The SnO_2 nanorods may also relieve the mechanical stress associated with the volume changes during the charging/discharging process.[65]

Charge transfer in Janus heterodimers has also been exploited for antimicrobial applications. For instance, the highly asymmetric Ag_2S–Ag heterodimers have exhibited strong bactericidal effects on *Escherichia coli* K-12 upon UV light irradiation.[66] The addition of Ag_2S–Ag heterodimers (0.01 mg mL^{-1}) under UV irradiation produced 3 times more units of inactivation of *E. coli* in 60 min compared with the system without UV light. If the Ag_2S–Ag concentration was increased to 0.10 mg mL^{-1}, the *E. coli* cells were completely inactivated within 50 min. The observed enhancement of photocatalytic activity of this bipolar composite was ascribed to easy evacuation of the lysates from the cells because a closed intracellular circuit loop was formed when UV energy was harvested with the surface-anchored Ag_2S–Ag heterodimers.

In a more recent study, Ag_2S−Ag heterodimer nanoprisms showed improved photocatalytic activity in the inactivation of *E. coil* cells under both visible and UV irradiation.[67] The Ag_2S−Ag nanoprisms were prepared by overgrowth of Ag on Ag_2S−Ag heterodimers from reactions between CdS and Ag^+ in the dark. Under visible-light irradiation, the complete inactivation of *E. coli* cells was achieved in 20 min, and in 5 min under UV irradiation. More importantly, the roles of heterodimers in the photocatalytic process were further understood. If *E. coli* cells were exposed to visible light for only 5 min, parts of the cell membranes became disintegrated; this suggests that the Ag_2S–Ag heterodimers can function as effective antennas for different incident photons in view of their outstanding photoabsorbing ability across the UV-visible to near-IR region to generate plasmonic "hot spots" at the corners of silver prisms that resulted in cell membrane degradation.

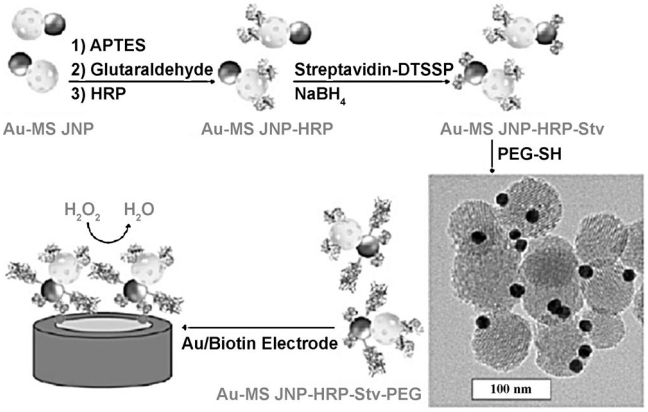

Figure 10. Schematic representation of the preparation of the Janus nanoparticle (JNP)-based biorecognition–signaling system and a representative TEM image of Janus Au−SiO_2 nanoparticles. Au−MS = Au–mesoporous silica, APTES = (3-aminopropyl)triethoxysilane, DTSSP = 3,3′-dithiobis(-sulfosuccinimidyl propionate). Reprinted with permission from ref. [69]. Copyright 2013 Elsevier.

4. Sensing Applications

Janus nanoparticles have also found extensive applications in chemical and biological sensing. A recent example demonstrates the potential of a designed Janus particle to incorporate therapeutic, targeting, and imaging modalities in one particle, in which one side of the particle is covered by a rough gold surface and the other side by polystyrene.[68] The polystyrene hemisphere can be selectively functionalized with ligands for targeting, whereas the gold film can be used for sensing or imaging that maximizes the efficacy of therapy through surface-enhanced Raman scattering (SERS). The Janus nanoparticles show effective targeting to breast cancer cells when anti-HER-2 antibodies are anchored on the polystyrene hemisphere surface and visualization of their interactions with cells is made possible through SERS detection of rhodamine 6G adsorbed on the rough gold surface.

In another study, Sánchez et al. described the applications of Janus nanoparticles as signaling elements for biorecognition in electrochemical biosensing.[69] Specifically, Janus gold–mesoporous silica nanostructures were prepared by masking mesoporous silica nanoparticles with paraffin wax followed by functionalization with (3-mercaptopropyl)trimethoxysilane attached to gold nanoparticles. The resulting Janus nanostructure was then functionalized with horseradish peroxidase (HRP) on the silica face, in which the gold surface was modified with streptavidin (Stv). Methoxypoly(-ethylene glycol) thiol (PEG-SH, MW = 5000) chains were also attached to the metal face to confer solubility to the nanoparticle. The Janus structure, Au-SiO_2-HRP-Stv-PEG, was observed by TEM, as shown in Figure 10.

To evaluate the biorecognition capability of the Janus Au-SiO_2-HRP-Stv-PEG nanostructures, electrochemical measurements were carried out with a biotin-modified gold disk electrode, onto which a film of Janus Au−SiO_2 was drop-cast. The interfacial changes on the gold electrodes after sequential modification with biotin and Janus Au-SiO_2-HRP-Stv-PEG nanostructures were analyzed by electrochemical impedance spectroscopy. Attachment of the modified nanoparticles led to more significant insulating effects on the electrode surface than that of control nanoparticles lacking Stv; this suggested higher specific adsorption of Au-SiO_2-HRP-Stv-PEG on the biotin-coated gold surface through the Stv motifs. Similar conclusions were reached from cyclic voltammetric measurements, which attended to the observed decrease in the peak currents and calculated electrochemical surface area after sequential modification of the electrode; this indicated that Janus Au-SiO_2-HRP-Stv-PEG had the ability to specifically biorecognize biotin residues on gold surfaces.

Furthermore, the capacity of this colloid to produce an enzyme-mediated electroanalytical signal was estimated by comparing the cyclic voltammetric responses of the Au/biotin/Janus Au-SiO_2-HRP-PEG and Au/biotin/Janus Au-SiO_2-HRP-Stv-PEG electrodes upon the addition of H_2O_2, for which an increase in the cathodic currents was observed at both modified electrodes. However, larger cathodic currents were observed in the electrode modified with Au/biotin/Au-MS JNP-HRP-Stv-PEG, which suggested that a larger amount of nanoparticles were adsorbed on the electrode and immobilized HRP electrocatalyzed the transformation of H_2O_2.

Janus gold nanoparticles have also been used as phase- and orientation-specific sensors for dopamine (DA).[70] Janus gold nanoclusters (2.6–5.0 nm in diam) were prepared by an in situ interfacial method by spreading a solution (50 μL) of a 1×10^{-3} M tetra-*n*-octylammonium tetrachloroaurate ([TOA][$AuCl_4$]) complex in chloroform with a Hamilton microsyringe onto the water surface of a LB trough (a calculated amount of tryptophan (0.01 mg mL^{-1}) was also added to the water subphase), followed by compression at a barrier speed of 5 mm min^{-1} to a desired surface pressure. The Janus gold nanoclusters were then deposited onto a glassy

carbon electrode by the Langmuir–Schaefer method under various surface pressures. Electronic communication between the nanoparticles may be controlled as a result of varied interparticle distances and sizes, which ultimately impact the sensitivity and detection limit of DA sensing. The apparent electron-transfer rate constants for DA detection suggested a detection limit in the sub-nanomolar range. The noncovalent interactions of the TOA^+ ligands and tryptophan in the monolayer arrays of the Janus gold nanoparticles further facilitated the electrocatalytic oxidation of DA, in which DA interacted with tryptophan at the nanoparticle surface through hydrogen-bonding interactions, thereby enhancing electrocatalytic oxidation at the particle-modified electrode. The presence of tryptophan at the peripheral Janus particle hemisphere attracted an increasing number of DA molecules towards the particle surface; thus enhancing the sensitivity thanks to the preconcentrating effects.

5. Summary and Perspectives

We have summarized some of the most commonly used methods for the preparation of Janus nanoparticles and highlighted their applications in electrochemistry, sensing, and photocatalysis. In general, the synthetic routes are based on interfacial engineering involving immobilization of the starting particles such that engineering and/or functionalization of the particles can be selected spatially. Whereas a variety of procedures have been developed for the preparation of (sub)micron-sized Janus particles, the leading methodologies in the synthesis of nanometer-sized amphiphilic Janus particles are largely based on Langmuir methods. With an asymmetric structure of the organically capping shell and/or the metal cores, Janus particles exhibit unique materials properties that are unseen with the homogeneously mixed counterparts, as highlighted in some recent studies with their enhanced electrocatalytic, photocatalytic, and biosensing activities.

Despite extensive progress in recent research, one major hurdle is the difficulty in scaling up the preparation of Janus particles. Thus, there is an urgent need in the development of more effective synthetic protocols. In addition, creation of more complicated patchy nanoparticles will be of great interest because the structures and properties of the particles may be manipulated at an unprecedented level, which will have a significant implication for nanoparticle-controlled assembly as well as spatially selective functionalization. Recently, Pons-Siepermann and Glotzer used computer simulations based on dissipative particle dynamics to predict the patterns of a mixed monolayer consisting of three thiol derivatives self-assembled on gold nanoparticle surfaces.[71] With deliberate variation of four critical parameters—nanoparticle core diameter, degree of ligand immiscibility, ligand chain length, and monolayer composition—they predicted the formation of varied patchy structures, including striped Janus particles as well as tri-patchy Neapolitan and Cerberus nanoparticles. In a recent study, we demonstrated experimentally,[72] for the first time, that trimetallic Ag@AuPt Neapolitan nanoparticles might be readily prepared by two-step galvanic exchange reactions at the two poles of silver nanoparticles. The results further demonstrate the effectiveness of interfacial engineering in the spatially selected functionalization of nanoparticles. It is anticipated that the ready availability of functional patchy nanoparticles will open up a new chapter in the study of nanoparticle surface functionalization and controlled assembly.

Acknowledgements

We thank the contributions of co-workers whose names are listed in the related references. This work was supported, in part, by the US National Science Foundation (DMR-0804049, CHE-1012258, CBET-1258839, and CHE-1265635).

[1] a) M. Brust, M. Walker, D. Bethell, D. J. Schiffrin, R. Whyman, *J. Chem. Soc. Chem. Commun.* **1994**, 801–802; b) P. D. Jadzinsky, G. Calero, C. J. Ackerson, D. A. Bushnell, R. D. Kornberg, *Science* **2007**, *318*, 430–433; c) H. Häkkinen, *Nat. Chem.* **2012**, *4*, 443–455.

[2] a) A. Perez, P. Melinon, V. Dupuis, L. Bardotti, B. Masenelli, F. Tournus, B. Prevel, J. Tuaillon-Combes, E. Bernstein, A. Tamion, N. Blanc, D. Tainoff, O. Boisron, G. Guiraud, M. Broyer, M. Pellarin, N. Del Fatti, F. Vallee, E. Cottancin, J. Lerme, J. L. Vialle, C. Bonnet, P. Maioli, A. Crut, C. Clavier, J. L. Rousset, F. Morfin, *Int. J. Nanotechnol.* **2010**, *7*, 523–574; b) A. Coskun, J. M. Spruell, G. Barin, W. R. Dichtel, A. H. Flood, Y. Y. Botros, J. F. Stoddart, *Chem. Soc. Rev.* **2012**, *41*, 4827–4859; c) R. P. Andres, J. D. Bielefeld, J. I. Henderson, D. B. Janes, V. R. Kolagunta, C. P. Kubiak, W. J. Mahoney, R. G. Osifchin, *Science* **1996**, *273*, 1690–1693; d) C. A. Berven, L. Clarke, J. L. Mooster, M. N. Wybourne, J. E. Hutchison, *Adv. Mater.* **2001**, *13*, 109–113.

[3] a) G. A. Somorjai, J. Y. Park, *Top. Catal.* **2008**, *49*, 126–135; b) V. Polshettiwar, R. S. Varma, *Green Chem.* **2010**, *12*, 743–754; c) N. Yan, C. X. Xiao, Y. Kou, *Coord. Chem. Rev.* **2010**, *254*, 1179–1218; d) H. Lee, C. Kim, S. Yang, J. W. Han, J. Kim, *Catal. Surv. Asia* **2012**, *16*, 14–27; e) C. Mohr, H. Hofmeister, J. Radnik, P. Claus, *J. Am. Chem. Soc.* **2003**, *125*, 1905–1911; f) L. N. Lewis, *Chem. Rev.* **1993**, *93*, 2693–2730.

[4] a) E. Katz, I. Willner, J. Wang, *Electroanalysis* **2004**, *16*, 19–44; b) S. W. Zeng, K. T. Yong, I. Roy, X. Q. Dinh, X. Yu, F. Luan, *Plasmonics* **2011**, *6*, 491–506; c) V. K. K. Upadhyayula, *Anal. Chim. Acta* **2012**, *715*, 1–18; d) S. Tokonami, Y. Yamamoto, H. Shiigi, T. Nagaoka, *Anal. Chim. Acta* **2012**, *716*, 76–91; e) S. R. Emory, W. E. Haskins, S. M. Nie, *J. Am. Chem. Soc.* **1998**, *120*, 8009–8010; f) M. Zayats, A. B. Kharitonov, S. P. Pogorelova, O. Lioubashevski, E. Katz, I. Willner, *J. Am. Chem. Soc.* **2003**, *125*, 16006–16014.

[5] J. F. Hainfeld, *Science* **1987**, *236*, 450–453.

[6] a) J. Kane, J. Ong, R. F. Saraf, *J. Mater. Chem.* **2011**, *21*, 16846–16858; b) S. H. Sun, C. B. Murray, D. Weller, L. Folks, A. Moser, *Science* **2000**, *287*, 1989–1992; c) T. Sun, K. Seff, *Chem. Rev.* **1994**, *94*, 857–870.

[7] G. Schmid, *Chem. Rev.* **1992**, *92*, 1709–1727.

[8] J. Z. Zhang, Z. L. Wang, J. Liu, S. W. Chen, G.-y. Liu, *Self-Assembled Nanostructures*, Kluwer, New York, **2003**.

[9] a) A. C. Templeton, M. P. Wuelfing, R. W. Murray, *Acc. Chem. Res.* **2000**, *33*, 27–36; b) M. G. Warner, S. M. Reed, J. E. Hutchison, *Chem. Mater.* **2000**, *12*, 3316–3320; c) R. Shenhar, V. M. Rotello, *Acc. Chem. Res.* **2003**, *36*, 549–561; d) H. Wellsted, E. Sitsen, A. Caragheorgheopol, V. Chechik, *Anal. Chem.* **2004**, *76*, 2010–2016; e) A. R. Rothrock, R. L. Donkers, M. H. Schoenfisch, *J. Am. Chem. Soc.* **2005**, *127*, 9362–9363.

[10] a) R. S. Ingram, M. J. Hostetler, R. W. Murray, *J. Am. Chem. Soc.* **1997**, *119*, 9175–9178; b) A. C. Templeton, D. E. Cliffel, R. W. Murray, *J. Am. Chem. Soc.* **1999**, *121*, 7081–7089.
[11] a) W. Chen, J. R. Davies, D. Ghosh, M. C. Tong, J. P. Konopelski, S. W. Chen, *Chem. Mater.* **2006**, *18*, 5253–5259; b) X. W. Kang, N. B. Zuckerman, J. P. Konopelski, S. W. Chen, *J. Am. Chem. Soc.* **2012**, *134*, 1412–1415.
[12] a) C. Casagrande, M. Veyssie, *C. R. Acad. Sci. Ser. II* **1988**, *306*, 1423–1425; b) P. G. de Gennes, *Science* **1992**, *256*, 495–497.
[13] A. Ulman, *An Introduction to Ultrathin Organic Films: From Langmuir–Blodgett to Self-Assembly*, Academic Press, Boston, **1991**.
[14] a) Z. Li, D. Lee, M. F. Rubner, R. E. Cohen, *Macromolecules* **2005**, *38*, 7876–7879; b) Z. Nie, W. Li, M. Seo, S. Xu, E. Kumacheva, *J. Am. Chem. Soc.* **2006**, *128*, 9408–9412.
[15] a) L. Hong, S. Jiang, S. Granick, *Langmuir* **2006**, *22*, 9495–9499; b) B. P. Binks, P. D. I. Fletcher, *Langmuir* **2001**, *17*, 4708–4710; c) T. Nisisako, T. Torii, T. Takahashi, Y. Takizawa, *Adv. Mater.* **2006**, *18*, 1152–1156.
[16] a) A. Perro, S. Reculusa, S. Ravaine, E. B. Bourgeat-Lami, E. Duguet, *J. Mater. Chem.* **2005**, *15*, 3745–3760; b) K. H. Roh, D. C. Martin, J. Lahann, *Nat. Mater.* **2005**, *4*, 759–763; c) D. Suzuki, H. Kawaguchi, *Colloid Polym. Sci.* **2006**, *284*, 1471–1476.
[17] V. N. Paunov, O. J. Cayre, *Adv. Mater.* **2004**, *16*, 788–791.
[18] a) J. Yoon, K. J. Lee, J. Lahann, *J. Mater. Chem.* **2011**, *21*, 8502–8510; b) F. Wurm, A. F. M. Kilbinger, *Angew. Chem.* **2009**, *121*, 8564–8574; *Angew. Chem. Int. Ed.* **2009**, *48*, 8412–8421; c) A. Walther, A. H. E. Mueller, *Soft Matter* **2008**, *4*, 663–668; d) S. Jiang, Q. Chen, M. Tripathy, E. Luijten, K. S. Schweizer, S. Granick, *Adv. Mater.* **2010**, *22*, 1060–1071; e) M. Lattuada, T. A. Hatton, *Nano Today* **2011**, *6*, 286–308; f) J. Du, R. K. O'Reilly, *Chem. Soc. Rev.* **2011**, *40*, 2402–2416; g) E. Duguet, A. Desert, A. Perro, S. Ravaine, *Chem. Soc. Rev.* **2011**, *40*, 941–960.
[19] a) J. R. Howse, R. A. L. Jones, A. J. Ryan, T. Gough, R. Vafabakhsh, R. Golestanian, *Phys. Rev. Lett.* **2007**, *99*, 048102–1; b) H. Takei, N. Shimizu, *Langmuir* **1997**, *13*, 1865–1868; c) O. Cayre, V. N. Paunov, O. D. Velev, *J. Mater. Chem.* **2003**, *13*, 2445–2450; d) Y. Lu, H. Xiong, X. C. Jiang, Y. N. Xia, M. Prentiss, G. M. Whitesides, *J. Am. Chem. Soc.* **2003**, *125*, 12724–12725.
[20] Z. N. Bao, L. Chen, M. Weldon, E. Chandross, O. Cherniavskaya, Y. Dai, J. B. H. Tok, *Chem. Mater.* **2002**, *14*, 24–26.
[21] a) L. Nagle, D. Ryan, S. Cobbe, D. Fitzmaurice, *Nano Lett.* **2003**, *3*, 51–53; b) S. G. Jang, S.-H. Kim, S. Y. Lee, W. C. Jeong, S.-M. Yang, *J. Colloid Interface Sci.* **2010**, *350*, 387–395.
[22] H. Y. Koo, D. K. Yi, S. J. Yoo, D. Y. Kim, *Adv. Mater.* **2004**, *16*, 274–277.
[23] a) R. Erhardt, M. F. Zhang, A. Boker, H. Zettl, C. Abetz, P. Frederik, G. Krausch, V. Abetz, A. H. E. Muller, *J. Am. Chem. Soc.* **2003**, *125*, 3260–3267; b) I. K. Voets, R. Fokkink, T. Hellweg, S. M. King, P. de Waard, A. de Keizer, M. A. C. Stuart, *Soft Matter* **2009**, *5*, 999–1005.
[24] a) J. Zhang, J. Jin, H. Zhao, *Langmuir* **2009**, *25*, 6431–6437; b) Z. Nie, D. Fava, E. Kumacheva, S. Zou, G. C. Walker, M. Rubinstein, *Nat. Mater.* **2007**, *6*, 609–614.
[25] a) D. Dendukuri, P. S. Doyle, *Adv. Mater.* **2009**, *21*, 4071–4086; b) R. F. Shepherd, J. C. Conrad, S. K. Rhodes, D. R. Link, M. Marquez, D. A. Weitz, J. A. Lewis, *Langmuir* **2006**, *22*, 8618–8622.
[26] Y. Wang, B.-H. Guo, X. Wan, J. Xu, X. Wang, Y.-P. Zhang, *Polymer* **2009**, *50*, 3361–3369.
[27] a) K. H. Roh, M. Yoshida, J. Lahann, *Langmuir* **2007**, *23*, 5683–5688; b) S. Hwang, K.-H. Roh, D. W. Lim, G. Wang, C. Uher, J. Lahann, *Phys. Chem. Chem. Phys.* **2010**, *12*, 11894–11899.
[28] F. Wurm, H. M. Koenig, S. Hilf, A. F. M. Kilbinger, *J. Am. Chem. Soc.* **2008**, *130*, 5876–5877.
[29] J. Zhang, X. Wang, D. Wu, L. Liu, H. Zhao, *Chem. Mater.* **2009**, *21*, 4012–4018.
[30] A. Perro, S. Reculusa, F. Pereira, M. H. Delville, C. Mingotaud, E. Duguet, E. Bourgeat-Lami, S. Ravaine, *Chem. Commun.* **2005**, 5542–5543.
[31] O. Cayre, V. N. Paunov, O. D. Velev, *Chem. Commun.* **2003**, 2296–2297.
[32] a) J. R. Millman, K. H. Bhatt, B. G. Prevo, O. D. Velev, *Nat. Mater.* **2005**, *4*, 98–102; b) M. Fialkowski, A. Bitner, B. A. Grzybowski, *Nat. Mater.* **2005**, *4*, 93–97.
[33] M. Yoshida, K. H. Roh, J. Lahann, *Biomaterials* **2007**, *28*, 2446–2456.
[34] B. P. Binks, S. O. Lumsdon, *Langmuir* **2001**, *17*, 4540–4547.
[35] a) S. C. Glotzer, *Science* **2004**, *306*, 419–420; b) Y. K. Takahara, S. Ikeda, S. Ishino, K. Tachi, K. Ikeue, T. Sakata, T. Hasegawa, H. Mori, M. Matsumura, B. Ohtani, *J. Am. Chem. Soc.* **2005**, *127*, 6271–6275.
[36] a) D. Suzuki, S. Tsuji, H. Kawaguchi, *J. Am. Chem. Soc.* **2007**, *129*, 8088–8089; b) S. C. Glotzer, M. J. Solomon, *Nat. Mater.* **2007**, *6*, 557–562.
[37] S. Berger, A. Synytska, L. Ionov, K.-J. Eichhorn, M. Stamm, *Macromolecules* **2008**, *41*, 9669–9676.
[38] R. A. Vaia, J. W. Lee, C. S. Wang, B. Click, G. Price, *Chem. Mater.* **1998**, *10*, 2030–2032.
[39] A. B. Pawar, I. Kretzschmar, *Macromol. Rapid Commun.* **2010**, *31*, 150–168.
[40] a) H. W. Gu, R. K. Zheng, X. X. Zhang, B. Xu, *J. Am. Chem. Soc.* **2004**, *126*, 5664–5665; b) Y. Q. Li, G. Zhang, A. V. Nurmikko, S. H. Sun, *Nano Lett.* **2005**, *5*, 1689–1692.
[41] S. Pradhan, L. P. Xu, S. W. Chen, *Adv. Funct. Mater.* **2007**, *17*, 2385–2392.
[42] L. P. Xu, S. Pradhan, S. W. Chen, *Langmuir* **2007**, *23*, 8544–8548.
[43] S. Pradhan, L. E. Brown, J. P. Konopelski, S. W. Chen, *J. Nanopart. Res.* **2009**, *11*, 1895–1903.
[44] K. F. Morris, A. L. Froberg, B. A. Becker, V. K. Almeida, J. Tarus, C. K. Larive, *Anal. Chem.* **2005**, *77*, 254A–263A.
[45] a) Y. Guo, M. G. Moffitt, *Macromolecules* **2007**, *40*, 5868–5878; b) O. Kohlmann, W. E. Steinmetz, X. A. Mao, W. P. Wuelfing, A. C. Templeton, R. W. Murray, C. S. Johnson, *J. Phys. Chem. B* **2001**, *105*, 8801–8809; c) X. Liu, M. Yu, H. Kim, M. Mameli, F. Stellacci, *Nat. Commun.* **2012**, *3*, 1182–1.
[46] a) A. M. Jackson, J. W. Myerson, F. Stellacci, *Nat. Mater.* **2004**, *3*, 330–336; b) A. M. Jackson, Y. Hu, P. J. Silva, F. Stellacci, *J. Am. Chem. Soc.* **2006**, *128*, 11135–11149.
[47] a) Q. Xu, X. W. Kang, R. A. Bogomolni, S. W. Chen, *Langmuir* **2010**, *26*, 14923–14928; b) S. Pradhan, D. Ghosh, S. W. Chen, *ACS Appl. Mater. Interfaces* **2009**, *1*, 2060–2065.
[48] a) M. W. Tsao, J. F. Rabolt, H. Schonherr, D. G. Castner, *Langmuir* **2000**, *16*, 1734–1743; b) G. Jeschke, P. Ionita, A. Volkov, V. Chechik, *Anal. Chem.* **2008**, *80*, 95–106.
[49] Y. Song, L. M. Klivansky, Y. Liu, S. Chen, *Langmuir* **2011**, *27*, 14581–14588.
[50] R. Shenhar, A. Sanyal, O. Uzun, V. M. Rotello, *Macromolecules* **2004**, *37*, 92–98.
[51] Z. W. Seh, S. Liu, M. Low, S.-Y. Zhang, Z. Liu, A. Mlayah, M.-Y. Han, *Adv. Mater.* **2012**, *24*, 2310–2314.
[52] X. Fu, J. Liu, H. Yang, J. Sun, X. Li, X. Zhang, Y. Jia, *Mater. Chem. Phys.* **2011**, *130*, 334–339.
[53] Z. W. Seh, S. Liu, S.-Y. Zhang, M. S. Bharathi, H. Ramanarayan, M. Low, K. W. Shah, Y.-W. Zhang, M.-Y. Han, *Angew. Chem.* **2011**, *123*, 10322–10325; *Angew. Chem. Int. Ed.* **2011**, *50*, 10140–10143.
[54] a) J. Lee, J. C. Park, H. Song, *Adv. Mater.* **2008**, *20*, 1523–1528; b) Y. Deng, Y. Cai, Z. Sun, J. Liu, C. Liu, J. Wei, W. Li, C. Liu, Y. Wang, D. Zhao, *J. Am. Chem. Soc.* **2010**, *132*, 8466–8473.
[55] X. Liu, C. H. Lee, W.-C. Law, D. W. Zhu, M. X. Liu, M. S. Jeon, J. H. Kim, P. N. Prasad, C. H. Kim, M. T. Swihart, *Nano Lett.* **2013**, *13*, 4333–4339.
[56] D. Rodríguez-Fernández, T. Altantzis, H. Heidari, S. Bals, L. M. Liz-Marzán, *Chem. Commun.* **2013**, *50*, 79–81.
[57] Y. Song, K. Liu, S. Chen, *Langmuir* **2012**, *28*, 17143–17152.
[58] C. Wang, W. Tian, Y. Ding, Y.-q. Ma, Z. L. Wang, N. M. Markovic, V. R. Stamenkovic, H. Daimon, S. Sun, *J. Am. Chem. Soc.* **2010**, *132*, 6524–6529.

[59] H. Yu, M. Chen, P. M. Rice, S. X. Wang, R. L. White, S. H. Sun, *Nano Lett.* **2005**, *5*, 379–382.
[60] F. Wang, S. Cheng, Z. H. Bao, J. F. Wang, *Angew. Chem.* **2013**, *125*, 10534–10538; *Angew. Chem. Int. Ed.* **2013**, *52*, 10344–10348.
[61] S. H. Choi, Y. C. Kang, *Nanoscale* **2013**, *5*, 4662–4668.
[62] a) H. Y. Koo, J. H. Yi, J. H. Kim, Y. N. Ko, D. S. Jung, Y. C. Kang, J.-H. Lee, *Mater. Chem. Phys.* **2010**, *124*, 959–963; b) M. Kim, R. M. Laine, *J. Am. Chem. Soc.* **2009**, *131*, 9220–9229.
[63] a) N. Zhao, M. Gao, *Adv. Mater.* **2009**, *21*, 184–187; b) A. Teleki, S. E. Pratsinis, K. Wegner, R. Jossen, F. Krumeich, *J. Mater. Res.* **2005**, *20*, 1336–1347; c) G. A. Sotiriou, A. M. Hirt, P.-Y. Lozach, A. Teleki, F. Krumeich, S. E. Pratsinis, *Chem. Mater.* **2011**, *23*, 1985–1992.
[64] a) C. Li, W. Wei, S. Fang, H. Wang, Y. Zhang, Y. Gui, R. Chen, *J. Power Sources* **2010**, *195*, 2939–2944; b) W. Xu, N. L. Canfield, D. Wang, J. Xiao, Z. Nie, J.-G. Zhang, *J. Power Sources* **2010**, *195*, 7403–7408.
[65] X. Ji, X. Huang, J. Liu, J. Jiang, X. Li, R. Ding, Y. Hu, F. Wu, Q. Li, *Nano. Res. Lett.* **2010**, *5*, 649–653.
[66] M. Pang, J. Hu, H. C. Zeng, *J. Am. Chem. Soc.* **2010**, *132*, 10771–10785.
[67] S. Xiong, B. Xi, K. Zhang, Y. Chen, J. Jiang, J. Hu, H. C. Zeng, *Sci. Rep.* **2013**, *3*, 2177–1.
[68] L. Y. Wu, B. M. Ross, S. Hong, L. P. Lee, *Small* **2010**, *6*, 503–507.
[69] A. Sánchez, P. Díez, P. Martínez-Ruíz, R. V. Villalonga, J. M. Pingarrón, *Electrochem. Commun.* **2013**, *30*, 51–54.
[70] P. Biji, A. Patnaik, *Analyst* **2012**, *137*, 4795–4801.
[71] I. C. Pons-Siepermann, S. C. Glotzer, *Soft Matter* **2012**, *8*, 6226–6231.
[72] Y. Song, S. W. Chen, *Nanoscale* **2013**, *5*, 7284–7289.

Received: October 18, 2013
Revised: November 15, 2013
Published online: December 27, 2013

